Precursor effect on Mn-Fe-Ce/TiO_2 catalysts for selective catalytic reduction of no with NH_3 at low temperatures

Putluru, Siva Sankar Reddy; Schill, Leonhard; Jensen, Anker Degn; Siret, Bernard; Tabaries, Frank; Fehrmann, Rasmus

Published in:
Catalysts

Link to article, DOI:
10.3390/catal11020259

Publication date:
2021

Document Version
Publisher's PDF, also known as Version of record

Citation (APA):
Putluru, S. S. R., Schill, L., Jensen, A. D., Siret, B., Tabaries, F., & Fehrmann, R. (2021). Precursor effect on Mn-Fe-Ce/TiO_2 catalysts for selective catalytic reduction of no with NH_3 at low temperatures. *Catalysts*, *11*(2), Article 259. https://doi.org/10.3390/catal11020259

catalysts

MDPI

Article

Precursor Effect on Mn-Fe-Ce/TiO_2 Catalysts for Selective Catalytic Reduction of NO with NH_3 at Low Temperatures

Siva Sankar Reddy Putluru [1], Leonhard Schill [1], Anker Degn Jensen [2], Bernard Siret [3], Frank Tabaries [3] and Rasmus Fehrmann [1,*]

1 Center for Catalysis and Sustainable Chemistry, Department of Chemistry, Building 207, Technical University of Denmark, DK-2800 Kgs. Lyngby, Denmark; sivasankarreddyp@gmail.com (S.S.R.P.); leos@kemi.dtu.dk (L.S.)
2 Combustion and Harmful Emission Control Research Center, Department of Chemical and Biochemical Engineering, Building 229, Technical University of Denmark, DK-2800 Kgs. Lyngby, Denmark; aj@kt.dtu.dk
3 LAB SA, 259 Avenue Jean Jaurés, 69364 CEDEX 07 Lyon, France; bernard.siret@lab.fr (B.S.); frank.tabaries@cnim.com (F.T.)
* Correspondence: rf@kemi.dtu.dk; Tel.: +45-45252389

Abstract: Preparation of Mn/TiO_2, Mn-Fe/TiO_2, and Mn-Fe-Ce/TiO_2 by the deposition-precipitation (DP) method can afford very active catalysts for low-temperature NH_3-SCR (selective catalytic reduction of NO with NH_3). The effect of precursor choice (nitrate vs. acetate) of Mn, Fe, and Ce on the physiochemical properties including thermal stability and the resulting SCR activity were investigated. The resulting materials were characterized by N_2-Physisorption, XRD (Powder X-ray diffraction), XPS (X-ray photoelectron spectroscopy), H_2-TPR (temperature-programmed reduction with hydrogen), and the oxidation of NO to NO_2 measured at 300 °C. Among all the prepared catalysts $5Mn_{Ace}$/Ti, $25Mn_{0.75Ace}Fe_{0.25Nit}$/Ti, and $25Mn_{0.75Ace}Fe_{0.20Nit}Ce_{0.05Ace}$/Ti showed superior SCR activity at low temperature. The superior activity of the latter two materials is likely attributable to the presence of amorphous active metal oxide phases (manganese-, iron- and cerium-oxide) and the ease of the reduction of metal oxides on TiO_2. Enhanced ability to convert NO to NO_2, which can promote fast-SCR like pathways, could be another reason. Cerium was found to stabilize amorphous manganese oxide phases when exposed to high temperatures.

Keywords: precursor effect; thermal stability; deposition-precipitation; NH_3-SCR of NO; MnFe/TiO_2

Citation: Putluru, S.S.R.; Schill, L.; Jensen, A.D.; Siret, B.; Tabaries, F.; Fehrmann, R. Precursor Effect on Mn-Fe-Ce/TiO_2 Catalysts for Selective Catalytic Reduction of NO with NH_3 at Low Temperatures. *Catalysts* **2021**, *11*, 259. https://doi.org/10.3390/catal11020259

Academic Editor: Soghomon Boghosian
Received: 20 January 2021
Accepted: 9 February 2021
Published: 15 February 2021

1. Introduction

NH_3-SCR (selective catalytic reduction of NO_x with NH_3) with V_2O_5-WO_3/TiO_2 as the catalyst is used successfully in stationary plants [1–5]. The support of choice is TiO_2 (anatase form) due to its higher surface area relative to rutile phase and the fact that SO_3 does not deteriorate the TiO_2 support. The commercial catalyst exhibits high selectivity and activity in the NH_3-SCR of NO at 300–400 °C [3–5]. In order to operate at this temperature, the SCR unit is usually installed at a high dust position.

However, by placing the SCR unit at the high dust position, the catalyst's life is shortened due to the high content of ash with alkali metals in the flue gas [6–8]. Therefore, the tail-end position, which is located behind the SO_2/SO_3-removing unit is attractive. Decreased erosion and fouling at the low dust level also increases the catalyst's lifetime [9]. In order to avoid costly reheating of the flue gas to around 350 °C, tail-end placement necessitates the SCR catalyst to be significantly more active than the vanadia-tungsta based one.

In recent years, a large number of research articles on NH_3-SCR of NO at low-temperature have been published. Among the reported catalysts, Mn/TiO_2 based formulations are the most promising [10,11]. Furthermore, bimetallic Mn catalysts showed higher activities and selectivities. Hence, Mn-Fe/TiO_2 [12–15], MnOx-CeO_2 [16], and Mn-Ce/TiO2 [17,18] have been reported to be highly active bimetallic catalysts for NH_3-SCR of

NO at low temperatures. Recently, we reported highly active low temperature Mn-Fe/TiO_2 catalysts prepared by deposition-precipitation using ammonia carbamate as a precipitating agent [19].

The low-temperature SCR activity of the MnO_x catalysts depends on the precursor, preparation method, and metal loading. Kapteijn et al. [20] reported that a Mn/Al_2O_3 catalyst was more active when prepared with Mn-acetate than with Mn-nitrate. Likewise, Li et al. [21] concluded that a Mn-acetate derived Mn/TiO_2 catalyst had better activity than its Mn-nitrate based version. However, Peña et al. [22] showed that a Mn/TiO_2 catalyst prepared from manganese nitrate and calcined at 400 °C had better activity at lower temperatures than a catalyst obtained from manganese acetate. Detailed investigation of the precursor effect on more active formulations like Mn-Fe/TiO_2 and Mn-Fe-Ce/TiO_2 catalysts has not been reported.

The optimum Mn loading of low temperature Mn/TiO_2 catalysts was reported to be 20 wt.% [22] while the optimum loadings of Mn and Fe in Mn-Fe/TiO_2 catalysts synthesized by impregnation were both 10 wt.% [14]. In our previous article [19], we reported that it was possible to further reduce the total metal loading on Mn/TiO_2 catalysts from 20 wt.% to 5 wt.% with a change in the method of synthesis from conventional impregnation to deposition, while the total metal loading of the Mn-Fe/TiO_2 catalysts could be reduced from 35 wt.% to 25 wt.%. Catalysts based on Mn-Fe/TiO_2 contain high amounts of active metals (about 20–25 wt.%) compared to the traditional V_2O_5-WO_3/TiO_2 system (about 7–10 wt.%). Additionally, unsupported manganese oxide in hollandite form [23] and MnOx-CeO_2 [16] exhibited high NH_3-SCR activity at low temperatures.

The present article deals with the preparation of Mn/TiO_2, Mn-Fe/TiO_2, and Mn-Fe-Ce/TiO_2 using several metal precursors. Various methods of characterization were employed to understand the differences in catalyst properties and activities.

2. Results and Discussion

The SCR NO conversion profiles of the $5Mn_{Nit}$ and $5Mn_{Ace}$ supported catalysts are shown in Figure 1. Among the catalysts studied, Mn deposited on TiO_2 showed superior catalytic activity followed by ZrO_2 and Al_2O_3. In particular, Mn_{Ace}/Ti was more active compared to the Mn_{Nit}/Ti. At 250 °C, the Mn_{Ace}/Ti and Mn_{Nit}/Ti catalysts displayed a NO conversion of 81 and 65%, respectively. The low temperature activity of the Mn/TiO_2 catalysts were compared with silica and alumina by Simirniotis et al. [24] and they concluded that Lewis acid sites, a high surface concentration of MnO_2, and good redox properties were important in achieving low temperature SCR activity. For further experiments, TiO_2 was chosen as the unique support.

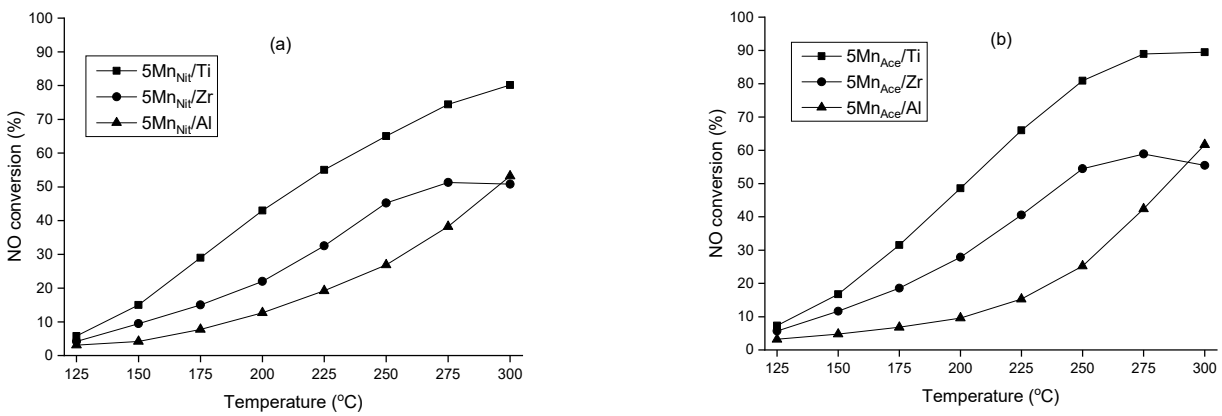

Figure 1. NO conversion profiles of: (**a**) $5Mn_{Nit}$ and; (**b**) $5Mn_{Ace}$ on various supports.

Mn/TiO_2 doped with transition metals (e.g., Ni, Cu, and Fe) had high resistance to sintering and more favorable Mn dispersion [12]. It is also reported that Mn/TiO_2 catalysts promoted with transition metals showed activity for NO oxidation to NO_2 [15].

In our previous publication, we reported the promotional effect of Fe on Mn/TiO_2 catalysts and the optimum formulation was found to be 25 $Mn_{0.75}Fe_{0.25}$/Ti using deposition-precipitation [19]. Figure 2a shows the NO conversion profiles of the 25 wt.% $Mn_{0.75}Fe_{0.25}$/Ti catalysts with Mn and Fe precursor combinations as a function of reaction temperature. All the catalysts, except for the $25Mn_{0.75Nit}Fe_{0.25Ace}$/Ti catalyst, showed full conversion above 225 °C. The $25Mn_{0.75Ace}Fe_{0.25Nit}$/Ti, $25Mn_{0.75Nit}Fe_{0.25Nit}$/Ti, $25Mn_{0.75Ace}Fe_{0.25Ace}$/Ti, and $25Mn_{0.75Nit}Fe_{0.25Ace}$/Ti catalysts exhibited NO conversion of 69.6, 55.6, 47.0, and 43.1% at 150 °C, respectively, illustrating the importance of precursors on catalyst activity.

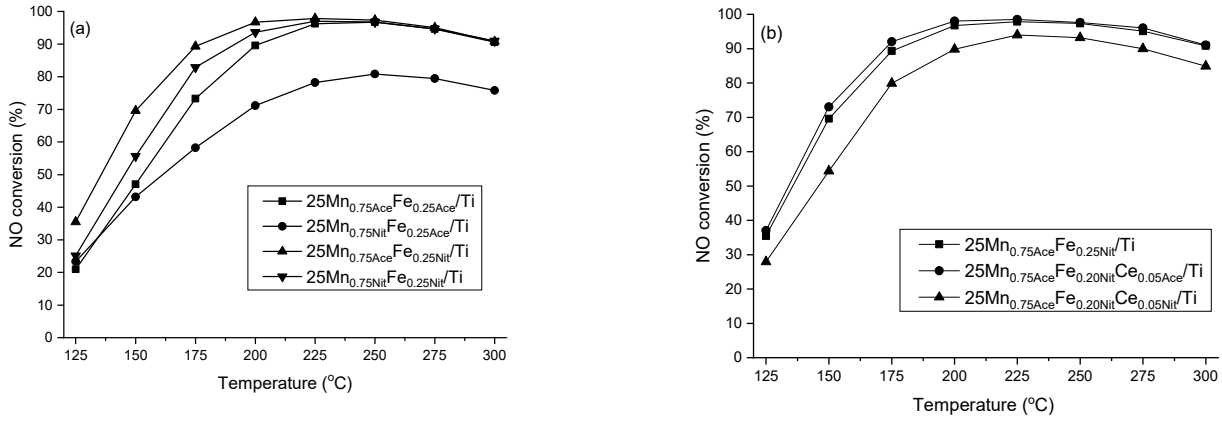

Figure 2. NO conversion profiles of catalysts prepared by different precursors: (**a**) $25Mn_{0.75}Fe_{0.25}$/Ti; (**b**) $25Mn_{0.75}Fe_{0.20}Ce_{0.05}$/Ti.

It is also well known that the presence of Ce can enhance the SCR performance and selectivity to N_2 [17]. It is also known that the presence of Ce further overcomes the SO_2 deactivation and water inhibition effects [18]. Figure 2b shows the effect of Ce precursor on the optimum $25Mn_{0.75Ace}Fe_{0.25Nit}$/Ti catalyst. The presence of Ce in the $25Mn_{0.75Ace}Fe_{0.20Nit}Ce_{0.05Ace}$/Ti catalyst showed slightly better performance while $25Mn_{0.75Ace}Fe_{0.20Nit}Ce_{0.05Nit}$/Ti showed less performance than the previously optimized $25Mn_{0.75Ace}Fe_{0.25Nit/}$Ti catalyst. This further confirms the sensitivity of SCR catalysts to the choice of precursors. The $25Mn_{0.75Ace}Fe_{0.25Nit}$/Ti, $25Mn_{0.75Ace}Fe_{0.20Nit}Ce_{0.05Ace}$/Ti, and $25Mn_{0.75Ace}Fe_{0.20Nit}Ce_{0.05Nit}$/Ti catalysts displayed NO conversions of 69.6, 73.0, and 54.4% at 150 °C, respectively. Table 1 summarizes the N_2O formation data obtained at 150 °C over the $25Mn_{0.75Ace}Fe_{0.25Nit}$/Ti, $25Mn_{0.75Ace}Fe_{0.20Nit}Ce_{0.05Ace}$/Ti, and $25Mn_{0.75Ace}Fe_{0.20Nit}Ce_{0.05Nit}$/Ti catalysts, which respectively produced 35, 15, and 20 ppm of N_2O under wet conditions (2.3 vol% H_2O). Thus, the presence of Ce can increase the selectivity to N_2. A moderate Ce content in Mn-Fe/TiO_2 catalysts contributed to decreased N_2O formation by hindering the over oxidation of NH_3, the dominant step in N_2O formation. N_2O formation is controlled by selective reaction of NO with NH_3, limiting the oxidation of NH_3. However, at a higher concentration of water (≈10 vol%), no N_2O was formed for all catalysts.

Table 1. N_2O formation data at 150 °C.

Catalyst	NO Conv. (%)	2.3 vol.% H_2O N_2O (ppm)	Sel. N_2O (%)	10 vol.% H_2O N_2O (ppm)	Sel. N_2O (%)
$25Mn_{0.75Ace}Fe_{0.25Nit}$/Ti	69.6	35	5.0	0	0
$25Mn_{0.75Ace}Fe_{0.20Nit}Ce_{0.05Ace}$/Ti	73.0	15	2.1	0	0
$25Mn_{0.75Ace}Fe_{0.20Nit}Ce_{0.05Nit}$/Ti	54.4	20	3.7	0	0

Figure 3a shows the NO conversion profiles of 20–30 wt.% $Mn_{0.75Ace}Fe_{0.20Nit}Ce_{0.05Ace}$/Ti catalysts vs. the reaction temperature. The NO conversion was in the following order: 25 $Mn_{0.75Ace}Fe_{0.20Nit}Ce_{0.05Ace}$/Ti > 20 $Mn_{0.75Ace}Fe_{0.20Nit}Ce_{0.05Ace}$/Ti > 30 $Mn_{0.75Ace}Fe_{0.20Nit}Ce_{0.05Ace}$/Ti

between 150–200 °C. Above 200 °C, the catalysts showed almost 100% NO conversion and it was not possible to discriminate between them. The 20, 25, and 30 wt.% $Mn_{0.75Ace}Fe_{0.20Nit}Ce_{0.05Ace}/Ti$ catalysts displayed a NO conversion of 59.8, 73.0, and 55.8% at 150 °C, respectively.

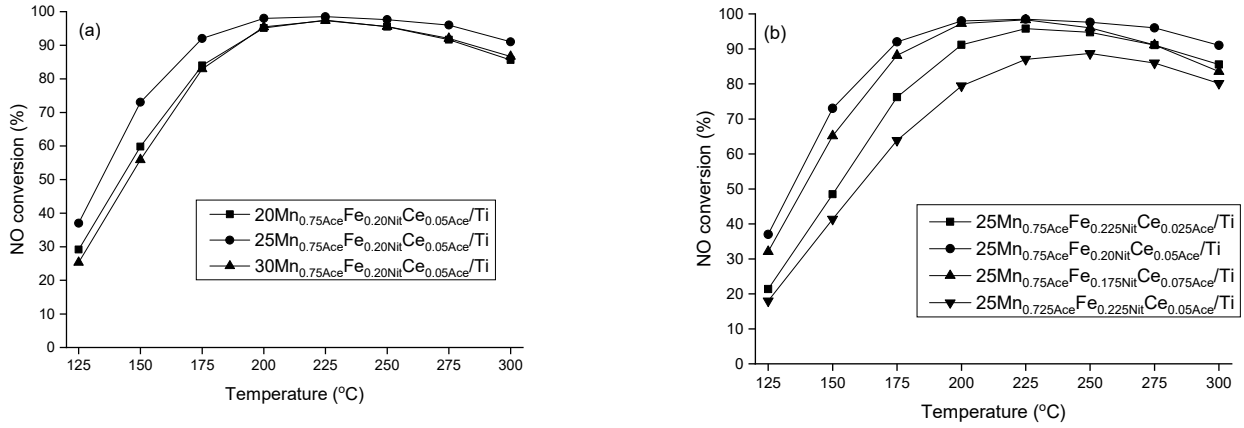

Figure 3. NO conversion profiles of: (**a**) 20–30 wt.% $Mn_{0.75Ace}Fe_{0.20Nit}Ce_{0.05Ace}/Ti$ catalysts; (**b**) $25Mn_{Ace}Fe_{Nit}Ce_{Ace}/Ti$ catalysts with $Mn_{0.75–0.725}$, $Fe_{0.225–0.175}$, $Ce_{0.075–0.025}$ mole fractions.

Figure 3b shows the SCR activity of the 25 wt.% $Mn_{Ace}Fe_{Nit}Ce_{Ace}/Ti$ catalyst with different Mn-Fe-Ce mole fractions. The highest NO conversion was attained at a Mn mole fraction of 0.75 and the lowest activity at a mole fraction of 0.725, indicating that the minimum Mn content should be 0.75. Maximum NO conversion was obtained at a Fe mole fraction of 0.20 followed by the mole fractions 0.175 and 0.225. Maximum NO conversion was obtained at a Ce mole fraction of 0.05 followed by 0.075 and 0.025. The $25Mn_{0.75Ace}Fe_{0.20Nit}Ce_{0.05Ace}/Ti$, $25Mn_{0.75Ace}Fe_{0.175Nit}Ce_{0.075Ace}/Ti$, $25Mn_{0.75Ace}Fe_{0.225Nit}Ce_{0.025Ace}/Ti$, and $25Mn_{0.725Ace}Fe_{0.225Nit}Ce_{0.05Ace}/Ti$ catalysts displayed NO conversions of 73.0, 65.2, 48.4, and 41.4 at 150 °C, respectively.

The effect of space velocity ($mLg^{-1}h^{-1}$) on the most active $25Mn_{0.75Ace}Fe_{0.20Nit}Ce_{0.05Ace}/Ti$ catalyst is shown in Figure 4. Space velocity is an important factor to be considered in the catalyst design as well as to compare to catalysts in the open literature. The catalyst displayed a NO conversion of 98, 88 and 79%, respectively, at space velocities of 360,000, 450,000, and 600,000 mL g^{-1} h^{-1} at 200 °C. The fact that at the lowest space velocity, NO conversions of above 90% can be attained at temperatures above 200 C indicates that unselective oxidation of NH_3 is not a major side reaction. The temperature window between 125 and 175 °C was used to determine an apparent activation energy of 38.6 ± 4.0 kJ/mol. This value clearly indicates that the present activity measurements on powdered samples were not strongly influenced by transport limitations in the pursued temperature window of the tail-end operation (125–175 °C).

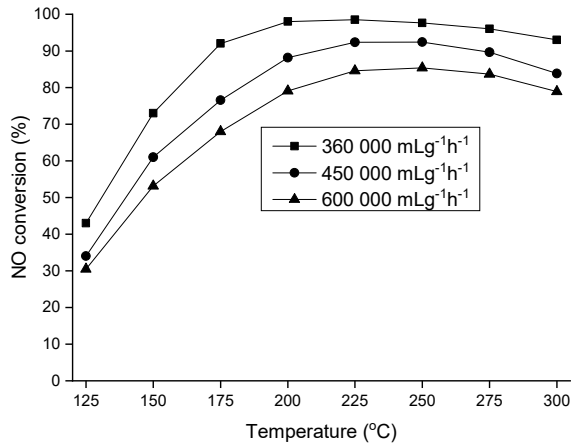

Figure 4. NO conversion profiles of the $25Mn_{0.75Ace}Fe_{0.20Nit}Ce_{0.05Ace}/Ti$ catalyst at various space velocities.

The BET (Brunauer–Emmett–Teller) surface area, H_2-TPR, and NO oxidation results of the MnFe/Ti and MnFeCe/Ti catalysts are summarized in Table 2. The BET surface area of DT51-TiO_2 was 83 m^2/g, while those of the MnFe/Ti and MnFeCe/Ti catalysts showed an increased surface area even with 25 wt.% active metal content. Thus, pore blockage of TiO_2 is unlikely and the active metal oxides are probably highly dispersed on the TiO_2 support. The increased surface area was due to increased microporosity compared to TiO_2 (see Figures S1 and S2, Supplementary Materials).

Table 2. Surface area, H_2-TPR (temperature-programmed reduction with hydrogen) and NO oxidation results.

Catalyst	Surface Area (m^2/g)	H_2 Consumption (μmol/g)	NO oxidation to NO_2 (%) *
$25Mn_{0.75Ace}Fe_{0.25Nit}/Ti$	95	4120	60
$25Mn_{0.75Nit}Fe_{0.25Nit}/Ti$	91	4004	58
$25Mn_{0.75Nit}Fe_{0.25Nit}/Ti$	100	3996	46
$25Mn_{0.75Nit}Fe_{0.25Ace}/Ti$	100	3972	42
$25Mn_{0.75Ace}Fe_{0.20Nit}Ce_{0.05Ace}/Ti$	102	5040	66
$25Mn_{0.75Ace}Fe_{0.20Nit}Ce_{0.05Nit}/Ti$	96	4907	56

* NO oxidation to NO_2 at 300 °C.

Ease of reduction of metals oxides is known to be an indicator for favorable low temperature SCR activity [19]. The H_2 consumption profiles of the 25MnFe/Ti and 25MnFeCe/Ti catalysts are shown in Figure 5 and the integrated values (μmol/g) are summarized in Table 2. All 25MnFe/Ti catalysts showed almost similar reduction patterns. To distinguish the bimetallic reduction patterns of the MnFe/Ti catalysts, the reduction patterns of Fe/TiO_2 and Mn/TiO_2 were reported [19]. The Fe/TiO_2 catalyst reduced from Fe_2O_3 to Fe at 338 °C. The Mn/TiO_2 catalyst showed three peaks corresponding to step-wise reduction of MnO_2 to Mn_2O_3, Mn_2O_3 to Mn_3O_4, and Mn_3O_4 to MnO [19]. The 25MnFe/Ti materials exhibited only two peaks with the first (maximum at ≈255–270 °C) corresponding to the MnO_2 reduction, and the second one (maximum at ≈350–390 °C) could be due to the reduction of subsequent manganese oxide phases mixed with iron oxide. The $25Mn_{0.75Ace}Fe_{0.25Ace}/Ti$ and $25Mn_{0.75Nit}Fe_{0.25Ace}/Ti$ catalysts showed visible shoulder peaks at around 230 and 340 °C, and that of the $25Mn_{0.75Ace}Fe_{0.25Nit}/Ti$ and $25Mn_{0.75Nit}Fe_{0.25Nit}/Ti$ catalysts did not display visible shoulder peaks because of the broad nature of the reduction profiles. The origin of the shoulder peak toward lower temperature is unclear, but might be because of the presence of smaller, more easily reducible manganese oxide particles.

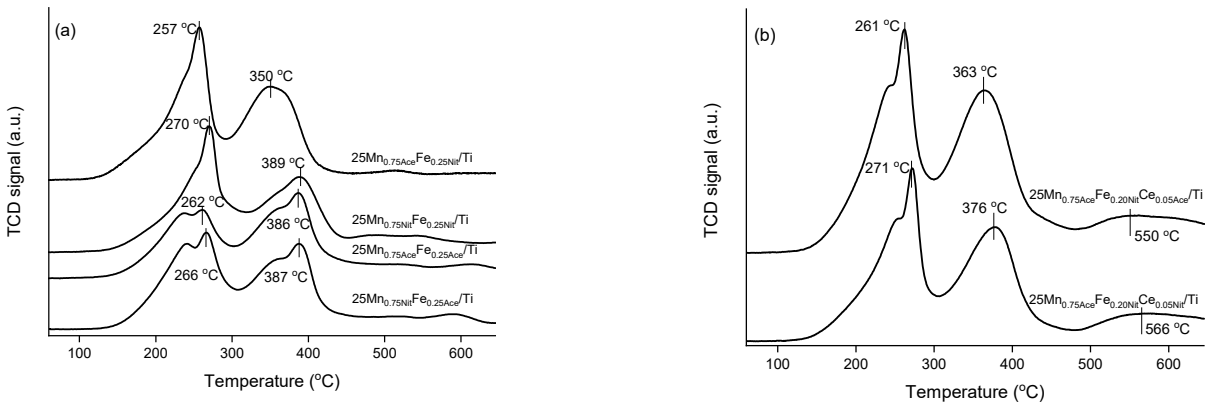

Figure 5. H_2-TPR (temperature-programmed reduction with hydrogen) profiles of (**a**) 25MnFe/Ti and (**b**) 25MnFeCe/Ti catalysts.

The $25Mn_{0.75Ace}Fe_{0.25Nit}/Ti$, $25Mn_{0.75Nit}Fe_{0.25Nit}/Ti$, $25Mn_{0.75Ace}Fe_{0.25Ace}/Ti$, and $25Mn_{0.75Nit}Fe_{0.25Ace}/Ti$ catalysts consumed 4120, 4004, 3996, and 3972 μmol/g of H_2, respectively. The difference in H_2 consumption between the catalysts was small, but the

$25Mn_{0.75Ace}Fe_{0.25Nit}$/Ti catalyst was reduced at a relatively low temperature. Thus, the ease of reduction pattern and the dominating MnO_2 phase (first peak) for the $25Mn_{0.75Ace}Fe_{0.25Nit}$/Ti catalyst seem to be the main contributors to the superior low temperature SCR activity.

The 25MnFeCe/Ti catalysts exhibited three reduction peaks, where the first two peaks can be assigned as similar to those of the MnFe/Ti catalysts and then the third reduction peak about 550 °C is due to the reduction of CeO_2 [25]. Most importantly, the $25Mn_{0.75Ace}Fe_{0.20Nit}Ce_{0.05Ace}$/Ti and $25Mn_{0.75Ace}Fe_{0.20Nit}Ce_{0.05Nit}$/Ti catalysts displayed a H_2 consumption of 5040 and 4907 μmol/g, respectively. This H_2 consumption, which is higher than for the 25MnFe/Ti catalysts, could be due to better dispersion of Mn, Fe, and Ce. The $25Mn_{0.75Ace}Fe_{0.20Nit}Ce_{0.05Ace}$/Ti catalyst was reduced at lower temperatures (≈10–15 °C) compared to the $25Mn_{0.75Ace}Fe_{0.20Nit}Ce_{0.05Nit}$/Ti catalyst. Thus, also in this case, the ease of reduction and the dominating MnO_2 phase (first reduction peak) in the $25Mn_{0.75Ace}Fe_{0.20Nit}Ce_{0.05Ace}$/Ti catalyst were the main reasons for the superior SCR activity at low temperature.

The X-ray powder diffraction (XRPD) patterns of the 25MnFe/Ti and 25MnFeCe/Ti catalysts are shown in Figure 6. The TiO_2 anatase phase was dominant in all catalysts and manganese oxide, iron oxide, and cerium oxides or other mixed phases of Mn, Fe, or Ce were not observed. This is a clear indication that active metal oxides are highly dispersed and/or in an amorphous state. To understand the amorphous state of the active metal oxides on the surface of the catalysts, thermal treatment at 400, 500, and 600 °C for 2 h was performed. It is anticipated that amorphous to crystalline phase transformation can happen by thermal treatment.

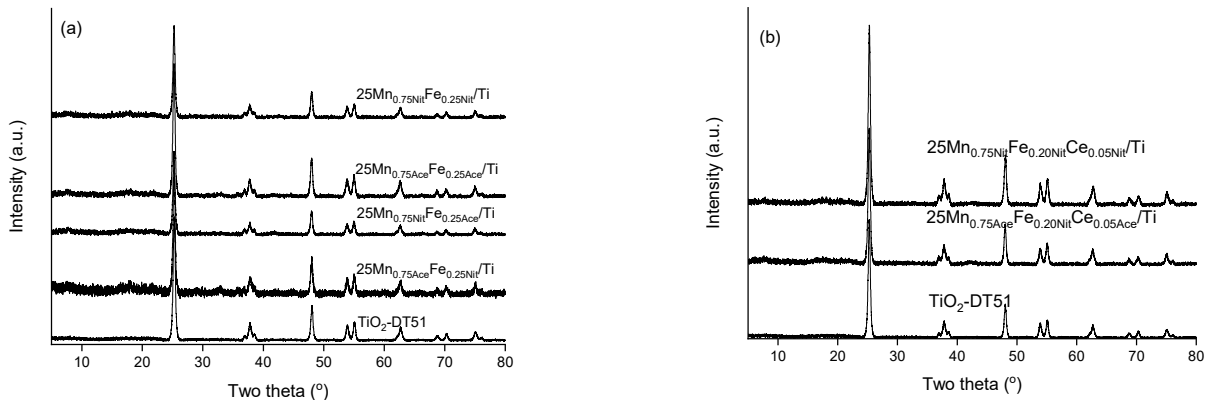

Figure 6. X-ray powder diffraction (XRPD) patterns of TiO_2 and the (**a**) 25MnFe/Ti and (**b**) 25MnFeCe/Ti catalysts.

The XRPD patterns of the 5MnAce/Ti, $25Mn_{0.75Ace}Fe_{0.25Nit}$/Ti, and $25Mn_{0.75Ace}Fe_{0.20Nit}$-$Ce_{0.05Ace}$/Ti samples calcined at several temperatures are shown in Figure 7. The 5MnAce/Ti catalyst showed similar diffraction patterns of anatase-TiO_2 at 400 °C and there was a small deviation compared to the TiO_2 patterns at 500 °C. With a further increase in temperature to 600 °C, MnO_2, Mn_2O_3, and anatase phases were observed. Similarly, the $25Mn_{0.75Ace}Fe_{0.25Nit}$/Ti catalyst showed only anatase phases of TiO_2 at 400 and 500 °C, and crystalline Mn_2O_3 and anatase TiO_2 phases were observed at 600 °C. No diffraction patterns of iron oxide were observed. Thus, we can clearly see that the presence of Fe can cause the transformation of the mixed manganese oxide phase into particles big enough for XRD detection to consist only of the Mn_2O_3 phase. The $25Mn_{0.75Ace}Fe_{0.20Nit}Ce_{0.05Ace}$/Ti catalyst showed only anatase TiO_2 phases even at 600 °C, thus the combined presence of Fe and Ce on Mn/Ti can hamper the transformation of the amorphous to the crystalline phase.

Figure 8 shows the NO conversion profiles of 5MnAce/Ti, $25Mn_{0.75Ace}Fe_{0.25Nit}$/Ti, and $25Mn_{0.75Ace}Fe_{0.20Nit}Ce_{0.05Ace}$/Ti catalysts calcined at 400, 500, and 600 °C. The catalysts were most active when calcined at 400 °C where the catalysts calcined at 500 and 600 °C showed lower activity. When calcined at 400 °C, the catalysts were rich in the amorphous metal oxide phases (manganese, iron or cerium oxides), which are known to be

SCR active. Further increase in calcination temperature resulted in the partial transformation of amorphous manganese oxide to crystalline manganese oxides (MnO_2 or Mn_2O_3). Overall, the SCR activity of the catalysts was in parallel to the amorphous to crystalline transformation of the catalysts as also reported by Kang and Tang et al. [26,27].

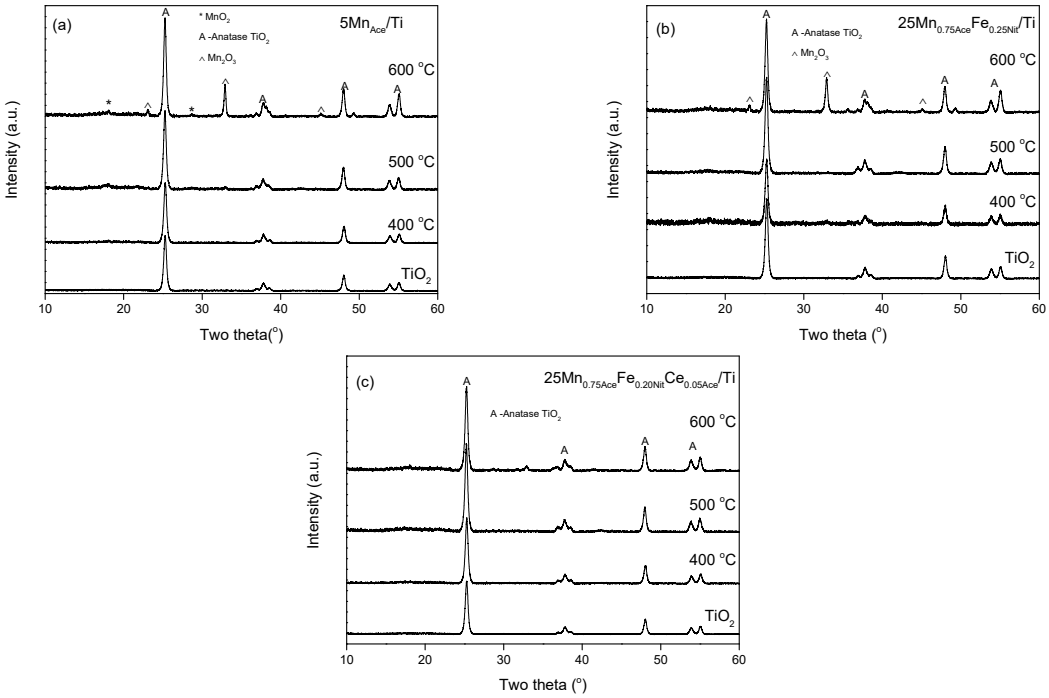

Figure 7. XRPD patterns of catalysts calcined at various temperatures: (**a**) 5MnAce/Ti; (**b**) $25Mn_{0.75Ace}Fe_{0.25Nit}/Ti$; (**c**) $25Mn_{0.75Ace}Fe_{0.20Nit}Ce_{0.05Ace}/Ti$.

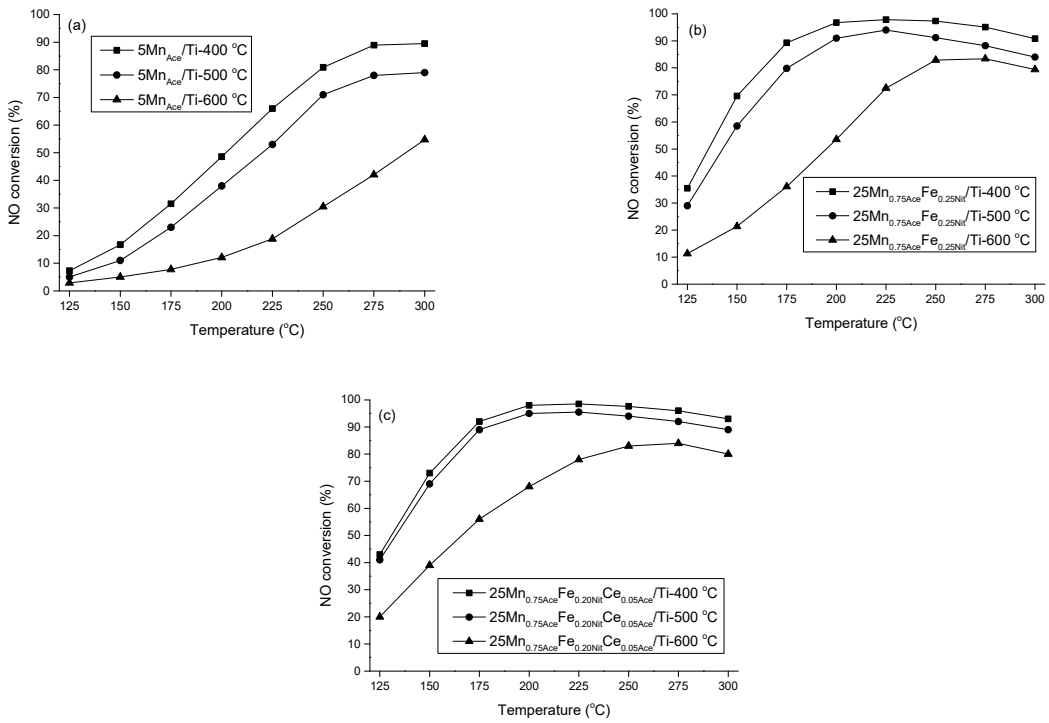

Figure 8. NO conversion profiles of catalysts calcined at various temperatures: (**a**) 5MnAce/Ti; (**b**) $25Mn_{0.75Ace}Fe_{0.25Nit}/Ti$; and (**c**) $25Mn_{0.75Ace}Fe_{0.20Nit}Ce_{0.05Ace}/Ti$.

The impact of the calcination temperature and transformation of active oxides can also be studied in combination with H_2-TPR. The redox properties of the 5MnAce/Ti, $25Mn_{0.75Ace}Fe_{0.25Nit}$/Ti, and $25Mn_{0.75Ace}Fe_{0.20Nit}Ce_{0.05Ace}$/Ti catalysts calcined at 400, 500, and 600 °C are shown in Figure 9. The 5MnAce/Ti catalyst showed three different reduction peaks, which correspond to stepwise reduction of MnO_2 to Mn_2O_3 (≈260 °C), Mn_2O_3 to Mn_3O_4 (≈360 °C), and Mn_3O_4 to MnO (≈460 °C) [19]. Increasing the calcination temperature from 400 to 600 °C, the 5MnAce/Ti catalyst shifted the first reduction peak to higher temperatures due to strong metal–support interactions [22], and the intensity of the second reduction peak was increased, which further indicates that the SCR active MnO_2 phase decreases and the Mn_2O_3 phase increases. The shifting of both reduction peaks to higher temperatures might be due to particle growth (sintering).

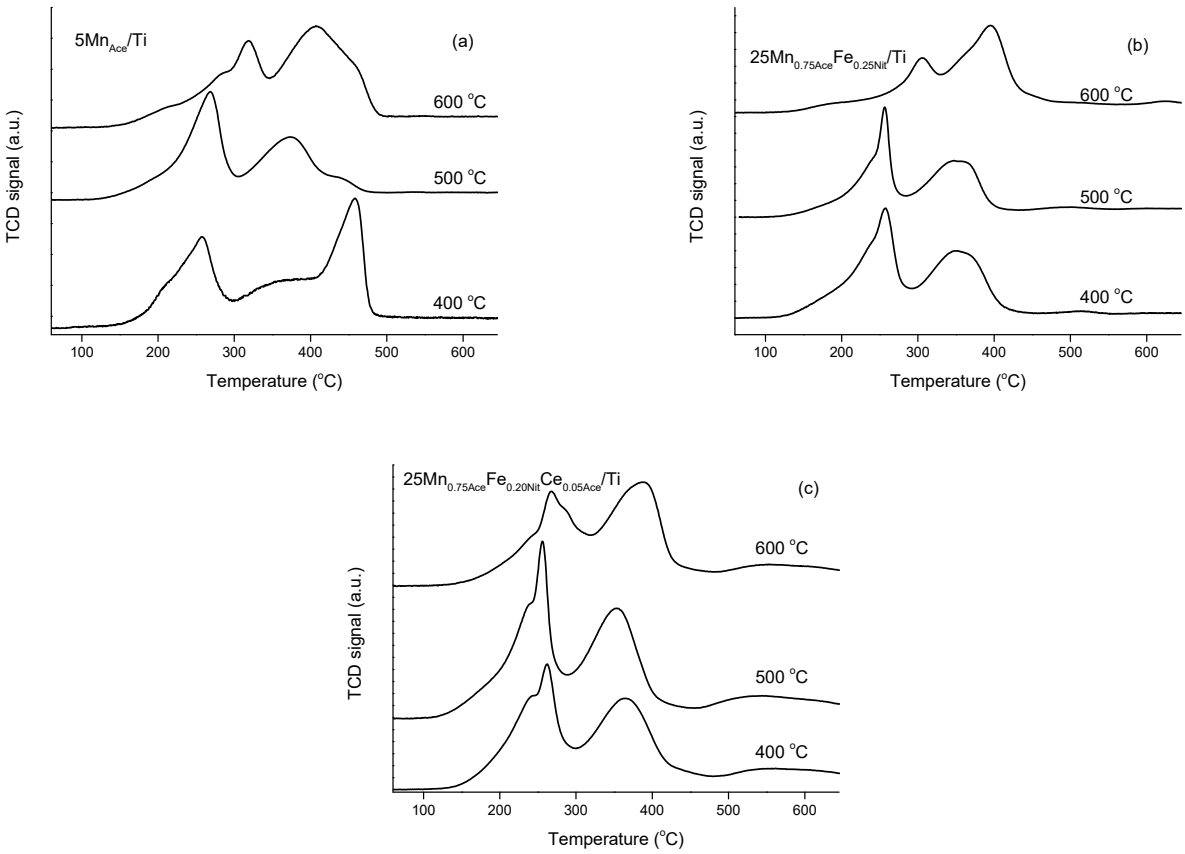

Figure 9. H_2-TPR (temperature-programmed reduction with hydrogen) profiles of catalysts calcined at various temperatures: (**a**) 5MnAce/Ti; (**b**) $25Mn_{0.75Ace}Fe_{0.25Nit}$/Ti; and (**c**) $25Mn_{0.75Ace}Fe_{0.20Nit}Ce_{0.05Ace}$/Ti.

The $25Mn_{0.75Ace}Fe_{0.25Nit}$/Ti and $25Mn_{0.75Ace}Fe_{0.20Nit}Ce_{0.05Ace}$/Ti catalysts showed almost similar reduction patterns at 400 and 500 °C of calcination temperature, further indicating that Fe and Ce are inhibiting the phase transformation of MnO_2 to Mn_2O_3 and possibly particle growth (sintering). At 600 °C, the catalyst displayed a shift in the MnO_2 reduction peak to high temperatures and the intensity of the second reduction peak was increased. Thus, the combined presence of Fe and Ce on Mn/TiO_2 can increase the thermal stability.

The observed low temperature activity of Mn catalysts can also be explained by the NO to NO_2 oxidation ability as reported previously [15,18]. Table 2 shows the oxidation of NO to NO_2 on the $25Mn_{0.75}Fe_{0.25}$Ti-DP and $25Mn_{0.75}Fe_{0.25}Ce_{0.05}$Ti-DP catalysts at 300 °C under wet conditions. All the catalysts displayed high NO to NO_2 conversion of 41.6 to 66%. The $25Mn_{0.75Ace}Fe_{0.20Nit}Ce_{0.05Ace}$/Ti and $25Mn_{0.75Ace}Fe_{0.25Nit}$/Ti catalysts displayed the highest NO to NO_2 conversion. The observed NO oxidation is consistent with the

increased SCR activity of the catalysts, since partial conversion of NO into NO_2 is helpful to promote the fast SCR reaction, which is also known to go on at very low temperatures [28].

The surface composition as obtained by XPS (X-ray photoelectron spectroscopy) characterization is shown in Table 3. The $25Mn_{0.75Ace}Fe_{0.25Nit}/Ti$ and $25Mn_{0.75Ace}Fe_{0.20Nit}Ce_{0.05Ace}/Ti$ showed a surface Mn/Fe molar ratio of 2.08 and 1.30, respectively. Thus, it appears that the precursor/promoter combination has an influence on forming MnFe oxide species on the surface of the support. Importantly, the $25Mn_{0.75Ace}Fe_{0.25Nit}/Ti$ catalyst showed an O_α concentration of 50.1% of the total oxygen while the Ce promoted $25Mn_{0.75Ace}Fe_{0.20Nit}Ce_{0.05Ace/}Ti$ catalyst yielded 83.8%, respectively. High concentrations of chemisorbed oxygen have been reported to have a beneficial influence on the low-temperature SCR reaction [12,29] and is explained by an increased rate of NO to NO_2 oxidation [29]. Our XPS results showed a significantly higher concentration of more reactive surface oxygen (O_α) in the $25Mn_{0.75Ace}Fe_{0.20Ni}tCe_{0.05Ace}/Ti$ catalyst than in the $25Mn_{0.75Ace}Fe_{0.25Nit}/Ti$ catalyst. This is reflected in the higher NO to NO_2 oxidation activity (66% vs. 60.4% conversion).

Table 3. Atomic% of MnFe/Ti and MnFeCe/Ti catalysts determined by XPS (X-ray photoelectron spectroscopy).

Catalyst	Ti	Mn	Fe	Ce	Mn/Fe	O_t	O_α/O_t
$25Mn_{0.75Ace}Fe_{0.25Nit}/Ti$	14.5	8.8	4.1	–	2.1	72.6	50.1
$25Mn_{0.75Ace}Fe_{0.20Nit}Ce_{0.05Ace}/Ti$	12.0	9.5	7.3	2.2	1.3	69.0	83.8

3. Experimental

3.1. Catalyst Synthesis

TiO_2 in anatase form (DT-51 from Crystal Global with a S content of ≈1.25 wt%, SA = 87 m^2g^{-1}), γ-Al_2O_3 (Saint-Gobain, surface area of 256 m^2/g), and ZrO_2 (Saint-Gobain, surface area of 95 m^2/g) were used as support materials. Manganese(II) nitrate tetrahydrate ($Mn(NO_3)_2 \cdot 4H_2O$, Aldrich), manganese (II) acetate tetrahydrate $(CH_3COO)_2Mn \cdot 4H_2O$, Aldrich), iron(III) nitrate nonahydrate ($Fe(NO_3)_3 \cdot 9H_2O$, Aldrich), iron(II) acetate ($Fe(CO_2CH_3)_2$, Aldrich), cerium (III) nitrate hexahydrate ($Ce(NO_3)_3 \cdot 6H_2O$, Aldrich), and Cerium (III) acetate hydrate ($Ce(CH_3CO_2)_3 \cdot xH_2O$, Aldrich) were used as precursors. The Mn/TiO_2, $Mn\text{-}Fe/TiO_2$, and $Mn\text{-}Fe\text{-}Ce/TiO_2$ catalysts were synthesized by deposition-precipitation. In deposition-precipitation (DP), the required amount of metal precursors (Mn, Fe, or Ce) and 1 g of support (TiO_2 or ZrO_2 or γ-Al_2O_3) was added to 10 mL demineralized water and mixed followed by the slow addition of ammonium carbamate solution (1 mol/L, Aldrich). The resulting slurry's aqueous phase was slowly removed by evaporation with continuous stirring followed by 12 h of oven treatment at 120 °C and finally calcined for 2 h in air at 400 °C. The catalysts were designated with total metal loading, metal composition, and metal precursor as 20–30 wt.% $Mn_{X\text{-}Ace}Fe_{Y\text{-}Nit}Ce_{Z\text{-}Ace}/Ti$, respectively. Here X, Y, and Z represent molar fractions of Mn, Fe, and Ce respectively (e.g., $25Mn_{0.75\text{-}Ace}Fe_{0.20\text{-}Nit}Ce_{0.05\text{-}Ace}/Ti$).

3.2. Catalyst Characterization

3.2.1. X-ray Powder Diffraction

X-ray powder diffraction (XRPD) was conducted with a Huber G670 instrument. CuKα radiation in steps of 0.02° was employed with a 2θ range of 2–60°. The Debye–Scherrer equation was used to calculate the crystallite sizes.

3.2.2. Nitrogen Physisorption

BET surface areas were determined from N_2 physisorption measurements on about 100 mg at 77 K with a Micromeritics ASAP 2010 apparatus. The samples were pretreated at 200 °C for 1 h before the measurement.

3.2.3. Chemisorption

H_2-TPR experiments were performed on a Micromeritics Autochem-II instrument with a reducing mixture (50 mL/min) consisting of 5% H_2 and balance Ar (Air Liquide)

from 60 to 550 °C (10 °C/min). The H_2 concentration in the effluent stream was monitored with a thermal conductivity detector (TCD).

3.2.4. X-ray Photoemission Spectroscopy

XPS measurements at room temperature were carried out with a Thermo scientific instrument. Al Kα radiation (1484.6 eV) was used and Au served as the standard for the instrument calibration. To minimize surface contamination, samples were outgassed in vacuum for 1 h in vacuum prior to the data acquisition. Deconvolution of spectra was performed using the Thermo Scientific Avantage Data system software.

3.3. Catalytic Activity Measurements

The SCR activity measurements were conducted in a fixed-bed reactor loaded with 50 mg of the fractionized (180–300 μm) catalyst at a flow rate of 300 NmL min^{-1} (at room temperature) at atmospheric pressure. The concentrations at inlet were: NO = 1000 ppm, NH_3 = 1000 ppm, O_2 = 4%, and H_2O = 2.3% with He as the make up gas. The temperature was increased from 125 to 300 °C in steps of 25 °C while the NO and NH_3 concentrations were measured continuously with a Thermo Electron Model 17C chemiluminescense NH_3-NOx analyzer. The N_2O concentration was measured by GC (Shimadzu 14 B GC, poraplot column, TCD detection). The concentrations were measured after reaching steady state conversion (approximately 45 min at each temperature).

The NO oxidation to NO_2 measurements were performed in the same set up loaded with 200 mg of the fractionized (180–300 μm) catalyst at a flow rate of 300 NmL min^{-1} (at room temperature). The inlet concentrations were: NO = 500 ppm, O_2 = 4.5% and H_2O = 2.3% with He as balance gas. During the experiments the temperature was increased in steps of 50 °C from 150 to 350 °C while the NO and NO_2 concentrations were measured with a Thermo scientific UV–Vis spectrophotometer (Evolution 220).

4. Conclusions

A range of precursor combinations in deposition-precipitation synthesis were tested on highly active low temperature SCR of NO with NH_3 catalysts. Among the three supports (TiO_2, ZrO_2, and Al_2O_3) and two precursor combinations (nitrate vs. acetate), a monometallic $5Mn_{Ace}$/Ti catalyst showed good low temperature SCR activity. Among the bimetallic catalysts, the $25Mn_{0.75Ace}Fe_{0.25Nit/}$Ti catalysts showed better low temperature SCR activity, and the trimetallic $25Mn_{0.75Ace}Fe_{0.20Nit}Ce_{0.05Ace/}$Ti catalyst showed the best low temperature SCR activity, respectively. The addition of Fe, and especially Ce, not only enhances the activity, but also the thermal stability by hindering the transformation of finely dispersed, easily reducible amorphous manganese oxide phases into larger, less easily reducible, and more crystalline particles as evidenced by H_2-TPR and XRD. Fe and Ce promoted catalysts were shown by XPS to contain large amounts of surface active oxygen, further corroborating the H_2-TPR and XRD results. This form of oxygen can enhance the oxidation of NO to NO_2, as shown by NO oxidation measurements, and can promote fast-SCR and hence the overall activity. Furthermore, Ce lowers the selectivity toward N_2O, possibly by enhancing the rate of reaction of activated NH_3 with NO to N_2, thus making it unavailable for over-oxidation, which can lead to N_2O formation.

Supplementary Materials: The following are available online at https://www.mdpi.com/2073-4344/11/2/259/s1, Figure S1: Adsorption/desorption isotherms of 25MnFe/Ti and 25MnFeCe/Ti catalysts with TiO_2 support. Figure S2: Cumulative surface area as a function of the BJH (Barrett-Joyner-Halenda) pore width (from adsorption branch) of the 25MnFe/Ti, 25MnFeCe/Ti catalysts and TiO_2 support.

Author Contributions: Conceptualization: S.S.R.P. and L.S.; Methodology: S.S.R.P., L.S.; R.F., and A.D.J.; Experimental: S.S.R.P. and L.S.; Writing of original draft: S.S.R.P.; Editing and reviewing of original draft: S.S.R.P., L.S., R.F., and A.D.J.; Revised draft: S.S.R.P. and L.S.; Project administration: R.F. and A.D.J.; Funding acquisition: R.F., B.S., and F.T.; Consulting from industrial point of view: B.S. and F.T. All authors have read and agreed to the published version of the manuscript.

Funding: This work was financially supported by Energinet.dk through the PSO project 10521. LAB S.A, France and DONG Energy, Denmark are also thanked for their financial support.

Data Availability Statement: The data generated in this study are fully disclosed in this manuscript.

Conflicts of Interest: The authors declare no conflict of interest. The funders had no role in the design of the study; in the collection, analyses, or interpretation of data; in the writing of the manuscript, or in the decision to publish the results.

References

1. Bosch, H.; Janssen, F. Formation and control of nitrogen oxides. *Catal. Today* **1988**, *2*, 369–379.
2. Parvulescu, V.I.; Grange, P.; Delmon, B. Catalytic removal of NO. *Catal. Today* **1998**, *46*, 233–316. [CrossRef]
3. Busca, G.; Lietti, L.; Ramis, G.; Berti, F. Chemical and mechanistic aspects of the selective catalytic reduction of NOx by ammonia over oxide catalysts: A review. *Appl. Catal. B* **1998**, *18*, 1–36. [CrossRef]
4. Alemany, L.J.; Lietti, L.; Ferlazzo, N.; Forzatti, P.; Busca, G.; Giamello, E.; Bregani, F. Reactivity and physicochemical characterization of V_2O_5-WO_3/TiO_2 De-NOx catalysts. *J. Catal.* **1995**, *155*, 117–130.
5. Heck, R.M. Catalytic abatement of nitrogen oxides-stationary applications. *Catal. Today* **1999**, *53*, 519–523. [CrossRef]
6. Due-Hansen, J.; Boghosian, S.; Kustov, A.; Fristrup, P.; Tsilomelekis, G.; Ståhl, K.; Christensen, C.H.; Fehrmann, R. Vanadia-based SCR catalysts supported on tungstated and sulfated zirconia: Influence of doping with potassium. *J. Catal.* **2007**, *251*, 459–473. [CrossRef]
7. Putluru, S.S.R.; Jensen, A.D.; Riisager, A.; Fehrmann, R. Heteropoly acid promoted V_2O_5/TiO_2 catalysts for NO abatement with ammonia in alkali containing flue gases. *Catal. Sci. Technol* **2011**, *1*, 631–637. [CrossRef]
8. Putluru, S.S.R.; Kristensen, S.B.; Due-Hansen, J.; Riisager, A.; Fehrmann, R. Alternative alkali resistant deNOx catalysts. *Catal. Today* **2012**, *184*, 192–196. [CrossRef]
9. Singoredjo, L.; Korver, R.; Kapteijn, F.; Moulijn, J. Alumina Supported Manganese Oxides for the Low-Temperature Selective Catalytic Reduction of Nitric-Oxide with Ammonia. *Appl. Catal. B Environ.* **1992**, *1*, 297–316. [CrossRef]
10. Smirniotis, P.G.; Peńa, D.A.; Uphade, B.S. Low-temperature selective catalytic reduction (SCR) of NO with NH3 by using Mn, Cr, and Cu oxides supported on Hombikat TiO_2. *Angew. Chem. Int. Ed.* **2001**, *40*, 2479–2482. [CrossRef]
11. Long, R.Q.; Yang, R.T.; Chang, R. Low temperature selective catalytic reduction (SCR) of NO with NH3 over Fe-Mn based catalysts. *Chem. Commun.* **2002**, *5*, 452–453. [CrossRef]
12. Wu, Z.; Jiang, B.; Liu, Y. Effect of transition metals addition on the catalyst for manganese/titania for low-temperature selective catalytic reduction of nitric oxide with ammonia. *Appl. Catal. B* **2008**, *79*, 347–355. [CrossRef]
13. Roy, S.; Viswanath, B.; Hegde, M.S.; Madras, G. Low-temperature selective catalytic reduction of NO with NH_3 over $Ti_{0.9}M_{0.1}O_2$-δ (M= Cr, Mn, Fe, Co, Cu). *J. Phys. Chem. C* **2008**, *112*, 6002–6012. [CrossRef]
14. Qi, G.; Yang, R.T. Low-temperature selective catalytic reduction of NO with NH3 over iron and manganese oxides supported on titania. *Appl. Catal. B Environ.* **2003**, *44*, 217–225. [CrossRef]
15. Wu, S.; Yao, X.; Zhang, L.; Cao, Y.; Zou, W.; Li, L.; Ma, K.; Tang, C.; Gao, F.; Dong, L. Improved low temperature NH3-SCR performance of FeMnTiOx mixed oxide with CTAB-assisted synthesis. *Chem. Commun.* **2015**, *51*, 3470–3473. [CrossRef]
16. Qi, G.; Yang, R.T.; Chang, R. MnOx-CeO_2 mixed oxides prepared by co-precipitation for selective catalytic reduction of NO with NH_3 at low temperatures. *Appl. Catal. B Environ.* **2004**, *51*, 93–106. [CrossRef]
17. Shang, T.; Hui, S.; Niu, Y.; Liang, L.; Liu, C.; Wang, D. Effect of the addition of Ce to MnOx/Ti catalyst on reduction of N_2O in low-temperature SCR. *Asia Pac. J. Chem. Eng.* **2014**, *9*, 810–817. [CrossRef]
18. Jin, R.; Liu, Y.; Wang, Y.; Cen, W.; Wu, Z.; Wang, H.; Weng, X. The role of cerium in the improved SO_2 tolerance for NO reduction with NH_3 over Mn-Ce/TiO2 catalyst at low temperature. *Appl. Catal. B Environ.* **2014**, *148–149*, 582–588. [CrossRef]
19. Putluru, S.S.R.; Schill, L.; Jensen, A.D.; Siret, B.; Tabaries, F.; Fehrmann, R. Mn/TiO_2 and Mn-Fe/TiO_2 catalysts synthesized by deposition precipitation-promising for selective catalytic reduction of NO with NH_3 at low temperatures. *Appl. Catal. B Environ.* **2015**, *165*, 628–635. [CrossRef]
20. Kapteijn, F.; Vanlangeveld, A.D.; Moulijn, J.A.; Andreini, A.; Vuurman, M.A.; Turek, A.M.; Jehng, J.M.; Wachs, I.E. Alumina-Supported Manganese Oxide Catalysts. *J. Catal.* **1994**, *150*, 94–104. [CrossRef]
21. Li, J.; Chen, J.; Ke, R.; Luo, C.; Hao, J. Effects of precursors on the surface Mn species and the activities for NO reduction over MnOx/TiO_2 catalysts. *Catal. Commun.* **2007**, *8*, 1896–1900. [CrossRef]
22. Peña, D.A.; Uphade, B.S.; Smirniotis, P.G. TiO_2-supported metal oxide catalysts for low-temperature selective catalytic reduction of NO with NH_3: I. Evaluation and characterization of first row transition metals. *J. Catal.* **2004**, *221*, 421–431. [CrossRef]

23. Huang, Z.; Gu, X.; Wen, W.; Hu, P.; Makkee, M.; Lin, H.; Kapteijn, F.; Tang, X. A "smart" hollandite deNOx catalyst: Self-protection against alkali poisoning. *Angew. Chem. Int. Ed.* **2013**, *52*, 660–664. [CrossRef]
24. Smirniotis, P.G.; Sreekanth, P.M.; Peña, D.A.; Jenkins, R.G. Manganese oxide catalysts supported on TiO_2, Al_2O_3, and SiO_2: A comparison for low-temperature SCR of NO with NH_3. *Ind. Eng. Chem. Res.* **2006**, *45*, 6436–6443. [CrossRef]
25. Thirupathi, B.; Smirniotis, P.G. Co-doping a metal (Cr, Fe, Co, Ni, Cu, Zn, Ce, and Zr) on Mn/TiO_2 catalyst and its effect on the selective reduction of NO with NH_3 at low-temperatures. *Appl. Catal. B Environ.* **2011**, *110*, 195–206. [CrossRef]
26. Kang, M.; Park, E.D.; Kim, J.M.; Yie, J.E. Manganese oxide catalysts for NOx reduction with NH_3 at low temperatures. *Appl. Catal. A Gen.* **2007**, *327*, 261–269. [CrossRef]
27. Tang, X.; Hao, J.; Xu, W.; Li, J. Low temperature selective catalytic reduction of NOx with NH_3 over amorphous MnOx catalysts prepared by three methods. *Catal. Commun.* **2007**, *8*, 329–334. [CrossRef]
28. Iwasaki, M.; Shinjoh, H. A comparative study of "standard", "fast" and "nO_2" SCR reactions over Fe/zeolite catalyst. *Appl. Catal. A Gen.* **2010**, *390*, 71–77. [CrossRef]
29. Shen, B.; Liu, T.; Zhao, N.; Yang, X.; Deng, L. Iron-doped Mn-Ce/TiO_2 catalyst for low temperature selective catalytic reduction of NO with NH_3. *J. Environ. Sci.* **2010**, *22*, 1447–1454. [CrossRef]